The Phase I Exclusive Physics at the Electron-Ion Collider: Opportunities at the ePIC Experiment

ePIC Exclusive Working Group*
(Dated: June 29, 2026)

The first five-year run of the Electron-Ion Collider (EIC), known as Phase I, marks the beginning of a new era in the study of the quantum chromodynamics (QCD). During this initial stage, the EIC will provide high-luminosity collisions of polarized electrons with protons and a variety of nuclear species, enabling a broad and foundational experimental program. This paper presents the strategy for the exclusive physics program with the ePIC experiment during Phase I. Utilizing the collider's high-luminosity polarized beams and state-of-the-art detection systems, ePIC is designed to probe the spatial and momentum distributions of partons inside nucleons and nuclei, explore the onset of gluon saturation, and investigate the spin structure of both free and bound nucleons. We describe initial detector performance, simulation studies, and analysis methodologies developed to tackle central questions in QCD. The Phase I program is expected to deliver critical benchmarks for the EIC's long-term scientific goals, advancing our understanding of hadronic structure and laying the foundation for future discoveries.

CONTENTS

* zhoudunming@bnl.gov; raphael.dupre@ijclab.in2p3.fr; stephen.kay@york.ac.uk

I. INTRODUCTION

The Electron-Ion Collider (EIC) is a next-generation particle accelerator currently under development at Brookhaven National Laboratory (BNL) in the United States. Designed as a cutting-edge facility for nuclear physics, the EIC will collide high-energy beams of polarized electrons with protons and atomic nuclei. This unique capability will allow scientists to explore the internal structure of matter with unprecedented precision, opening new windows into the fundamental structure of visible matter—particularly its strongly interacting nature, as described by the theory of Quantum Chromodynamics (QCD).

At the heart of the EIC's mission is the goal of imaging the internal structure of nucleons (protons and neutrons) and nuclei in terms of their quark and gluon constituents. Unlike previous accelerators, the EIC will provide high luminosity, a wide range of center-of-mass energies and nuclear species, and full control over the polarization of both the electron and hadron (proton and helium-3) beams. These features will enable precise measurements of parton distribution functions (PDFs), transverse momentum-dependent PDFs (TMDs), and generalized parton distributions (GPDs), offering multidimensional insight into how quarks and gluons generate the mass, spin, and internal dynamics of hadrons. Fundamental questions—such as the origins of mass and spin—are expected to be addressed by the EIC.

The EIC will also shed light on how gluons—the force carriers of the strong interaction—behave inside nuclei, and whether their densities saturate at high energies, as predicted by QCD. Understanding this gluon-dominated regime, sometimes referred to as the Color Glass Condensate, is essential for building a complete picture of nuclear matter under extreme conditions. Beyond its core physics goals, the EIC will serve as a powerful platform for technological innovation, workforce development, and international scientific collaboration, shaping the future of high-energy nuclear science.

To tackle the unprecedented challenges posed by QCD, the current strategy is to proceed step by step, requiring careful planning of a detailed experimental program. Given the complexity of operating a new collider facility, the plan is to run collisions with protons and various ions during the first five years—referred to as Phase I of the EIC—with an emphasis on both machine commissioning and early high-impact physics results. This will provide critical experience in operating the collider at its full range of energies and in ramping up to its design luminosity.

In this paper, we assess the physics program of the Phase I EIC using state-of-the-art Monte Carlo generators, which are fully simulated through the ePIC detector. The goal is to provide a first quantitative estimate of the scientific impact achievable within the initial five years of operation. We discuss both the expected physics outcomes and what will remain out of reach during Phase I. Given the broad scope of EIC science, this paper focuses specifically on the exclusive, diffractive, and tagged physics programs. Furthermore, as the field is rapidly evolving, we limit our discussion to a few highly selective processes, with follow-up studies anticipated.

The paper is structured as follows: Section II provides a brief introduction to the ePIC detector. Given the limited number of published resources on ePIC, only an overview is presented, with further details referenced from existing documentation and the ePIC website. Section III introduces the kinematics of Deep Inelastic Scattering (DIS) and defines all relevant variables. As no experimental data are yet available, all physics studies are based on simulations with Monte Carlo generators, discussed in Section IV. Section V outlines the detailed running conditions of the first five years at the EIC. Backgrounds from both physics processes and machine effects are briefly addressed in Section VI, followed by physics projections in Section VII. Our conclusion is presented in Section VIII.

II. DETECTOR

The ePIC detector is designed with the primary goal of providing hermetic and high-precision tracking, excellent vertex resolution, and broad calorimetric coverage to reconstruct a wide array of final-state particles. It must cope with the asymmetric beam energies of the EIC (e.g., 18 GeV electrons on 275 GeV protons) and the resulting boosted kinematics, which require efficient detection across both the forward and backward regions. To this end, the detector features a central solenoidal system with a magnetic field of 1.7 Tesla for precise tracking and momentum measurement, complemented by forward and backward subsystems for measuring electrons, hadrons, and forward nuclear fragments.

A. the ePIC detector

Key components of the ePIC detector include a silicon vertex tracker (Monolithic Active Pixel Sensor - MPAS []) for precision tracking near the interaction point, a central and forward tracking system with Multi Pattern Gas Detectors (MPGDs) and AC-LGAD sensors for low momentum particles, electromagnetic and hadronic calorimeters, a dedicated particle identification system using time-of-flight and Cherenkov detectors, beamline detectors for diffractive and exclusive measurements in the far-forward hadron-going region, and luminosity monitor and low-Q^2 taggers for small scattering-angle outgoing electrons. Additionally, the detector is designed with flexibility in mind, allowing upgrades or modifications to target specific physics topics as the EIC evolves. For details of these designs, see the official ePIC website (https://www.epic-eic.org/) for reference.

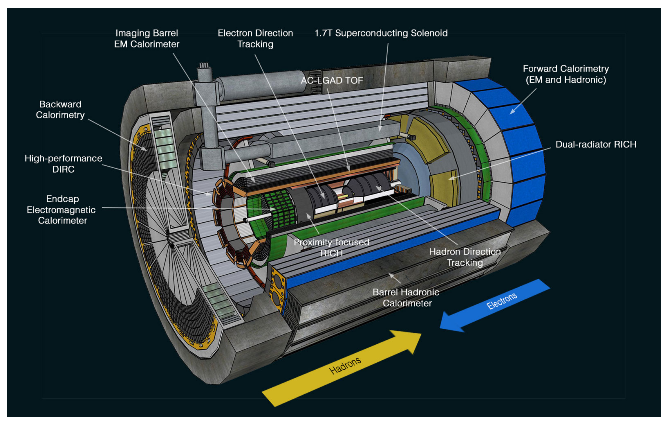

FIG. 1: The ePIC main detector cutaway view. (to be updated for the original file)

B. Far-forward beamline detector system

The ePIC far-forward detectors are required to enable essentially the entirety of the exclusive physics program at the EIC, where final-states involve protons, neutrons, photons, and various other particles at $\eta > 4.5$. There are four subsystems, all integrated with the outgoing hadron beamline between ∼5.5 and 39 meters from the interaction point. The far-forward subsystems, which have B0 detector, Roman Pots (RP), off-momentum detector (OMD), , and the zero degree calorimeter (ZDC), shown in Fig. 2.

The B0 detector is embedded in the magnet bore, which contains two sub-detectors: a charged particle tracker and an electromagnetic calorimeter. Both will have acceptance covering the angular region from 5.5 to 20 mrad. Given the mechanical constraints imposed by the detectors' location in the magnet (and respecting the beam lines themselves) the detectors will be highly asymmetric for angles greater than $\sim$13 mrad. The primary goal of the B0 detector is to accept forward going charged particles, mostly protons, and photons.

The Roman pots (RP) and off-momentum detector (OMD) subsystems are both intended to tag far-forward protons and reconstruct their momenta. These detectors are based on the same technology. Specifically, measurement of protons with scattering at angles < 5 mrad requires tracking detectors integrated directly into the outgoing hadron beamline. In previous and current experiments, silicon detectors meeting these basic criteria have been implemented in the form of Roman pots (RP) subsystems, and the EIC will take a similar approach.

However, since the ePIC experiment will also aim to tag and reconstruct protons which arise from the breakup of light nuclei (deuterons, helium-3, etc.), another set of silicon detectors which are optimally placed for capturing these protons is required. These off-momentum detectors (OMD) enable tagging and reconstruction of spectator protons whose momentum is significantly smaller than that of the hadron beam itself. We classify the various far-forward protons based on their magnetic rigidity, which determines their trajectories through the seven magnets (four dipoles for bending/steering; three quadrupoles for focusing) between the interaction point and the drift region where the RP and OMD systems are located.

For the sake of simplicity, the ratio of the longitudinal momentum of the proton with the total momentum of the beam itself is used to determine if the proton is within the RP or OMD fiducial acceptance, and defined as $x_L = p_{z,proton}/p_{beam}$. As an example, a proton from the breakup of a deuteron has an $x_L \sim 50\%$, on average. The RP acceptance is for $x_L > 65\%$, while the OMD covers a region between $25\% \lesssim x_L \lesssim 65\%$, with the lower bound being determined heavily by the scattering angles in question, since low-x_L particles will not follow the design beam orbit and will often be lost in the magnets before reaching the OMD. The RP and OMD are placed to have a small overlap in x_L to aid in alignment of the detectors, and calibration of the matrices used to reconstruct the particle's momentum.

Finally, the ZDC is designed to detector neutral forward particles, which must achieve energy and polar-angle resolutions for neutron showers better than $50\%/\sqrt{E}$ and $3\,\text{mrad}/\sqrt{E}$ as specified in the Yellow Report [1]. For electromagnetic showers, it must achieve $20\%/\sqrt{E}$ resolution [? ?]. The ZDC also needs to tag photons in the $\mathcal{O}(10\text{–}100\,\text{MeV})$ range in eA collisions.

These requirements originate from the extensive physics program enabled by the ZDC in ep, ed, eH^3 and

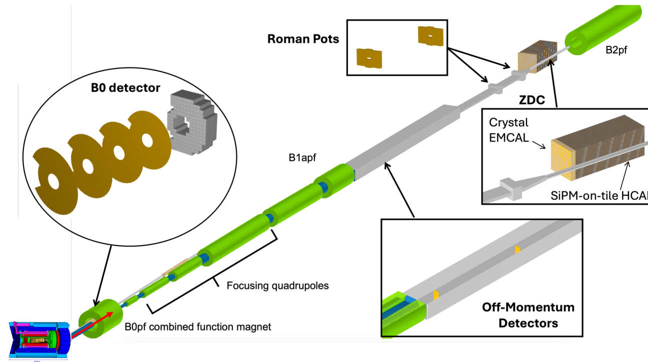

FIG. 2: All four far-forward subsystems in the outgoing hadron beam direction. The green cylinders are accelerator dipole and quadrupole magnets.

eA collisions that need measurements of neutral particles such as neutrons, photons, neutral pions, neutral lambda baryons, and other neutral mesons and baryons at near-zero polar angle with respect to the hadron beam. Summary of the Far-Forward detector systems is shown in Table. I.

III. KINEMATICS

In ePIC experiment at the EIC, the event kinematics can be categorized in a few ways: i) inclusive DIS variables, ii) tagging DIS variables, iii), diffractive variables, and iv) exclusive variables.

A. DIS variables

The DIS kinematics are characterized by the negative four-momentum transfer squared at the electron vertex, $Q^2 = -q^2 = -(e-e')^2$, the Bjorken-x, $x_{Bj} = Q^2/(2p\cdot q)$, and the inelasticity $y = (p\cdot q)/(p\cdot e)$. Here, e, e',p, and q denote the four-momenta of the incident electron, scattered electron, incoming nucleon, and exchanged photon, respectively. The center-of-mass energy $W_{\gamma N}$ between the virtual photon and the nucleon is given by $W^2_{\gamma N} = (p+q)^2$. Techniques of reconstructing these inclusive kinematic variables are discussed in [2].

B. Tagging variables

Generally, we study the spectator tagging process with proton or neutron detection in the final state from the nuclear breakup. For simplicity we write the following formulas for the case of proton detection; the formulas for neutron detection can be obtained by simple exchange $p \leftrightarrow n$. Note that the proton detections are mostly done by the B0 spectrometer and OMD, while neutrons are

Detectors	(x,z) Positions [m]	Dimensions	θ [mrad]	Notes
B0 tracker	$(x = 0.19,\ 5.4 < z < 6.4)$	(26 cm, 27 cm, n/a)	$5.5 < \theta < 20$	13 mrad at $\phi = \pi$
Off-momentum	(0.8, 22.5),(0.85,24.5)	(30 cm, 30 cm, n/a)	$0 < \theta < 5.0$	40% to 60% rigidity
Roman Pots	(0.85, 26.0), (0.94, 28.0)	(25 cm, 10 cm, n/a)	$0 < \theta < 5.0$	10σ cut
ZDC	(0.96, 37.5)	(60 cm, 60 cm, 2 m)	$0 < \theta < 5.5$	~ 4.0 mrad at $\phi = \pi$

TABLE I: Summary of the physical location, maximum polar angular acceptance for the four far-forward detectors [1]. this needs to be updated!

detected in the ZDC which has very different energy and momentum resolution.

For this paper, the tagging variables are mostly used in the case of deuteron spectator tagging. For details, see Ref. [3]. Specifically, there are two spectator kinematic variables for spectator proton (thus the subscript p): i) $p_{p\mathrm{T}}$ and ii) light-cone momentum fraction α_p.

- $p_{p\mathrm{T}}$ is the transverse momentum of the spectator in the lab frame.
- $\alpha_p = 1 + \frac{k^z}{E(\boldsymbol{k})}$, where $\mathbf{k}$ is the three-momentum of the spectator in the ion rest frame and $E(k)$ is the corresponding energy $\sqrt{|k|^2 + M_N^2}$. For deuteron, $0 < \alpha_p < 2$ where the longitudinal momentum of a spectator nucleon is bound by the total momentum of the deuteron.

Similar definitions can be derived for higher A nuclei. The case of neutron detection is described by the same formulas with $p \to n$.

C. Diffractive variables

In experimental terms, diffractive processes are identified by the presence of a rapidity gap — a region in the detector with no particle activity. These processes were extensively studied at HERA, where they were interpreted using the concept of *Pomeron exchange*. The Pomeron is modeled as a color-singlet object composed of two gluons with zero spin, mediating the interaction between the virtual photon (emitted by the electron) and the hadron.

The key kinematic variables used to describe diffraction are:

- $x_P = \frac{x}{\beta}$: the fraction of the hadron's momentum carried by the Pomeron;
- $t = -(p' - p)^2$: the squared four-momentum transfer between the initial (p) and final (p') hadron states;
- $\beta = \frac{Q^2}{Q^2 + M_X^2 - t}$: where Q^2 is the virtuality of the photon and M_X^2 is the invariant mass squared of the diffractive hadronic system.

To analyze diffractive events, one needs the standard DIS kinematic variables (x and Q^2), along with measurements of the momentum transfer t and the properties of the final-state hadronic system. A crucial experimental signature is the presence of a rapidity gap and/or the direct detection of the scattered hadron. In cases where the diffractive final state M_X consists of a single particle or a well-defined state, the process is referred to as an *exclusive reaction*, reflecting the constrained and clean event topology.

D. Exclusive variables

Specifically, exclusive reactions refer to processes in which the entire final state of particles is detected, enabling precise reconstruction of the reaction dynamics. The "exclusivity" of such reactions imposes stringent requirements on detector acceptance. In these events, the scattered proton or nucleus typically loses only a small fraction of its momentum and often escapes undetected through the beam pipe. Ensuring exclusivity therefore relies on dedicated forward detection systems, including the far forward proton spectrometer, which consists of components such as the B0 detector, Roman pots, off-momentum detectors, and the zero-degree calorimeter (used for detecting neutral particles). Once exclusivity is established, it becomes essential to measure the relevant kinematic variables with high precision and broad acceptance. Of particular importance is the distribution of the momentum transfer t, which plays a key role in the imaging program.

There are several methods to reconstruct the momentum transfer variable t, each offering distinct advantages depending on the specific reaction under study. A convention for the various methods of t-reconstruction was outlined following discussions at the 2025 ePIC collaboration meeting in Frascati, Italy [**?**]. In this convention, the 4-momenta of final states are generically defined as:

- p^μ_{BA}: outgoing **BA**ryon 4-momentum.
- p^μ_{BE}: incoming proton **BE**am momentum.
- $p^\mu_{\gamma^*}$: difference between incoming and scattered electron 4-momenta. I.e. information relating to $\mathbf{e}$ and e'

- p_X^μ: 4-momentum of the rest of final state, **X**.

and t can be calculated using using combinations of this information. This is included in the subscript of the t reconstruction method. For example, t_{BABE} utilizes the outgoing baryon (BA) information and the incoming proton beam (BE). In the case of deeply virtual Compton scattering (DVCS) on a proton, t_{BABE} corresponds directly to Equation. **??**. The reconstruction of p' can be based on B0 and/or the roman pots, where p is the nominal incoming proton beam momentum. The detector where p' might be reconstructed varies as $-t$ increases and the beam energy combination changes as can be seen clearly in Figure. **??**, which also demonstrates the resolution of t reconstruction from some of the far forward detector systems. Equally, t_{eX} for DVCS would be the reconstruction of t utilizing only the incoming and scattered electron information (e) and the final state γ (X).

Each method offers distinct advantages depending on the specific reaction under study. In practice, it is often beneficial to combine these approaches or use partial information from each to enhance the accuracy of t-reconstruction. This flexibility becomes especially important in regions of phase space where certain methods are limited or inapplicable—for example, when the outgoing heavy nucleus is not detectable.

Beyond the more conventional reconstruction methods, further improvements can be made by exploiting the differences among them to suppress events with poor resolution, though this comes at the cost of reduced statistics. Another recent proposal suggests reconstructing the momentum transfer t along a specific projected direction to mitigate the impact of detector smearing [4]. This approach can be used in conjunction with, and as an enhancement to, the traditional methods outlined above. Such developments are particularly crucial for the imaging program of heavy nuclei at the highest collision energies at the EIC.

IV. MONTE CARLO GENERATORS

- **PYTHIA 8** PYTHIA simulates high-energy particle collisions based on the framework of Quantum Chromodynamics (QCD) and electroweak theory, capturing both perturbative and non-perturbative aspects of the interactions. The simulation begins with a hard scattering process between partons (quarks or gluons), calculated using perturbative QCD matrix elements. This is followed by parton showers, where initial- and final-state radiation accounts for the emission of additional gluons and quarks due to QCD bremsstrahlung, approximated using DGLAP evolution equations. As the partons evolve and separate, hadronization occurs via the Lund string model, where color field lines between partons stretch into strings that eventually break into color-neutral hadrons. PYTHIA also includes models for multiparton interactions (MPI) and beam remnants, which are especially important at high energies. The result is a full event record of particles that reflects both the quantum field theoretical dynamics and the complex structure of the colliding hadrons.

- **Sartre** A Monte Carlo model for gluon saturation physics via exclusive VM photo- and electro-production in photon-nucleus collisions. The model applies nonlinear gluon evolution to calculate the scattering amplitude of a color-dipole, provided by the photon, and a target at a given impact parameter. Based on the Good-Walker paradigm, the model can predict both coherent and incoherent VM production, where the coherent process probes the average gluon density and the incoherent process is sensitive to the density fluctuation. Also known as the hot-spot model, the mechanism in incoherent VM production implements fluctuations of the parton and nucleon positions inside of a nucleon and a nucleus, respectively, their gluon densities, and their associated saturation scale Q_s. For this analysis, the comparisons to the measured data are based on Refs. [5, 6]. This model is only valid for parton momentum fraction $x_{\text{parton}} < 0.01$, while it is compared with the STAR data at $x_{\text{parton}} \approx 0.03$. The small mismatch to the data's kinematics needs to be taken into account when interpreting the data.

- **BeAGLE** A general-purpose electron-nucleus (e+A) model, BeAGLE [7] is used for the description of incoherent photoproduction only. Details of this model are given in Refs. [3, 7–10]. The comparison to heavy-ion (A+A) UPC cross sections is done by correcting the photon flux from e+A to A+A, where the e+A photon flux is based on PYTHIA 6 [11] and the A+A UPC photon flux is provided by the STARlight generator. BeAGLE uses the FLUKA program [12, 13] to describe neutron emission from nuclei. For this analysis, the comparisons to the measured data are based on Ref. [7].

- **DEMPgen** DEMPgen is a modular event generator for **D**eep **E**xclusive **M**eson **P**roduction reactions [14]. DEMPgen utilizes parameterizations of theoretical model to produce absolutely-normalized event samples. This enables a quick and direct projection of event rates. DEMPgen is capable of producing events in both fixed target and colliding beam kinematics. In collider kinematics, events for the DEMP reaction $p(e, e'\pi^+n)$, of interest for pion form factor studies, up to a Q^2 of 35 GeV^2. This kinematic range is limited by the current parametrization of Regge-based models utilized in the event generator.

Upgrades to DEMPgen, including the expansion of this Q^2 range, are ongoing.

- **lAger** known as Argonne Generic l/A Event Generator is a highly adaptable and modular Monte Carlo simulation framework developed to model a broad range of lepton- and photon-induced reactions on both nucleons and complex nuclei [15]. Designed with versatility in mind, lAger supports simulations across a wide kinematic regime, encompassing both fixed-target configurations, typical of experiments at facilities such as Jefferson Lab, and collider geometries, such as those envisioned for the upcoming EIC. Significant recent development has focused on enhancing the capabilities of lAger to support Deeply Virtual Meson Production (DVMP) processes, which are of central importance in probing the partonic structure of hadrons and nuclei via GPDs. The generator has been adapted to incorporate models for exclusive vector meson production, with specific attention given to the production of heavy quarkonia such as the J/ψ. Studies of J/ψ production have primarily focused on the kinematic regime defined $1 < Q^2 < 10$ GeV^2, which is particularly relevant for probing the transition between non-perturbative and perturbative QCD dynamics.

- **EpIC** EpIC [16, 17] is a state-of-the-art Monte Carlo event generator developed for the study of exclusive processes. It is built on the PARTONS platform [18, 19], which provides a modular and extensible software architecture, allowing for the integration of a wide range of theoretical models describing the partonic structure of the nucleon. EpIC currently supports a range of exclusive reactions, including Deeply Virtual Compton Scattering (DVCS), Time-like Compton Scattering (TCS), Deeply Virtual Meson Production (DVMP) with π^0, and Double Deeply Virtual Compton Scattering (DDVCS). It also features the implementation of radiative corrections. EpIC is well-suited for both the analysis of existing experimental data and for impact studies, particularly in the context of future experiments at EIC [20].

V. PHASE I EIC RUNNING SCHEMES

The initial planning of the Phase I EIC is summarized in Table. II. The setup is based on both the physics impact and the early commissioning of the newly built accelerator machine. That said, the plan may be subject to change depending on the development of the project as well as the interest from the ePIC collaboration. For now, we make physics projection studies based on this table only.

Working through this table from top to bottom, there are opportunities for exclusive, diffractive and tagging measurements in each stage. For running using electron-ion collisions with silver nuclei at 9x115, the primary The primary physics focus during this period is on (diffractive) DIS on nuclei. This will lay the groundwork for future precision studies on the gluon saturation phenomenon - which was also one of the "*Day 1*" measurements from the EIC White Paper.

Measurements from 9x130 collisions involving unpolarized deuterons and longitudinally polarized electrons include spectator-tagged DIS. This channel is crucial for measuring the free neutron's structure. 9x130 collisions with longitudinal electrons on transversely polarized protons will be instrumental for processes that probe nucleon and meson structure. These processes include deeply virtual Compton scattering (DVCS), deeply virtual meson production (DVMP), and deeply exclusive meson production (DEMP). Further 9x130 electron-proton collisions with longitudinally polarized protons will provide further statistics for nucleon and meson structure studies. The combination of beam polarizations can be leveraged to perform spin-dependent measurements, which will further study the proton spin decomposition, especially the quark and gluon Orbital Angular Momentum.

Electron-gold collisions at 9x100 will enable the study of nuclear effects in exclusive processes. One such process is diffractive vector meson production which will provide insights into the gluon spatial distribution in heavy nuclei. Collisions with helium-3 at 9x166 with longitudinal electrons along with transverse or longitudinal helium-3 will enable studies of DIS spectator tagging to measure the spin-dependent structure function of the neutron. These studies are essential for studying the partonic structure of nuclei and nucleons.

VI. ANALYSIS TECHNIQUES, BACKGROUNDS, AND UNCERTAINTY

For most of the ePIC physics analyses, scattered electron is reconstructed not only for the DIS kinematic variables, but also physics variables. The exception may be the photoproduction process, which we do not discuss in this paper. Specifically for the exclusive physics program, the event activities/occupancies in the main ePIC detector are very low, mostly 1-2 particles. The general event selection will be as follows:

- Good scattered electron candidates that satisfy i) $0.8 < E/p < 1.2$ and ii) $18 < E - P_z < 22$ GeV or similar (need to update from Win). Depending on analyses, the scattered electron can be reconstructed via a combination of EEMC cluster for energy measurement and tracking for the momentum measurement. Particle Identification (PID) detectors are not used in this study, which is expected to further improve the electron purity.

Species	Beam energy (GeV)	Integrated luminosity (fb^{-1})	Electron-beam polarization	Hadron-beam polarization
e+Ag	9×115	1.0	NO	N/A
e+D	9×130	1.5	LONG	NO
$e+p$	9×130	1.0	LONG	TRANS and/or LONG
$e+p$	9×275	2.5	LONG	TRANS and/or LONG
e+Au	9×100	1.0	LONG	N/A
$e+{}^3$He	9×166	1.5	LONG	TRANS and/or LONG

TABLE II: EIC early science matrix. The $e + A$ luminosity is per nucleon.

- Phase space selection on x, y, W, and/or Q^2.
- Event activity or multiplicity is limited to only the exclusive final-state, e.g., $N_{track} < 3$ for exclusive ϕ meson production. In addition, for proton beams, missing mass cut is also placed to further improve the exclusive event purity and resolutions.
- For protons and light ion beams, far-forward detectors will reconstruct the scattered protons and nucleons from nuclear breakup, respectively. We require a B0, RP, or OMD track by ensuring at least one hit per layer in their respective subsystem. (details will need to be flushed out).
- For heavy nuclei, event rejection by veto activities in the FF system is used. We reverse the selection criteria for each subsystem in the FF above, and we require none of them has a signal track in order to veto this event.

In the current studies, we estimate the impact from residue inclusive DIS events that survive our exclusive event selections. It is found that the exclusivity selection mostly has a purity of more than 95% (to be updated), depending on the final-state, as shown in Table III. For example, the DVπ^0P channel exhibits negligible DIS background contamination at low t, whereas the contamination increases to approximately 60% at high t after accounting for cross-section weighting within the available statistics. A larger simulated sample is required to quantify this effect more reliably and to draw definitive conclusions. Furthermore, events with resonances in the final state, e.g., vector-meson, generally has even higher exclusive event efficiency due to the selection on the mass. For instance, the DVMP with J/ψ can have a residue DIS background where low multiplicity events that proton can be excited and become neutron However, the exception is the eAu diffractive ϕ production where the dominate background comes from incoherent ϕ production. The remaining background events is on the order of 1% but its highly t dependent. See results later in Section VII.

In addition, DVπ^0P can be a physics background to DVCS when the two photons from the π^0 decay are reconstructed as a single photon. The corresponding misidentification probability is estimated to be at most ∼1% for the 5×41 GeV beam configuration and is expected to be significantly lower at the higher energies relevant for early science operation.

For DVCS and DVπ^0P, the impact from machine backgrounds, including contributions from synchrotron radiation, electron Bremsstrahlung, electron Touschek scattering, electron Coulomb scattering, and proton beam-gas interaction, is also estimated. The background photons are mixed with the signals, but the purity of π^0 for DVπ^0P is 96% thanks to its mass window cut.

	DIS & machine background contamination (Q^2 >1 GeV^2)
DVCS	3% for DIS and < 1% from π^0
DVπ^0P	0% low t and 60-100% for high t
DEMP	0.012% for DIS
DVMP	<40% but can be removed by mass fits
eAu ϕ	∼1% incoherent
eHe3	Photoproduction (not studied here)

TABLE III: Current estimates of contamination from DIS event and machine (all sources - beam gas, synchrotron etc) backgrounds for all of the exclusive, diffractive and tagging analyses described in this section.

At the current stage, since no ePIC detector system is built, estimating systematic uncertainties based on the instrumentation can be difficult and unrealistic. Therefore, our approach is to evaluate systematic uncertainty in a limited fashion, with either projected performance of a detector or uncertainties related to the analysis from previous experiences, e.g., HERA. Below are a few major uncertainty sources that are currently under consideration:

- Integrated luminosity - 1%
- Event and track selections
- Selection on signal extraction
- Incoherent diffractive contamination
- ...

In Table. IV, the dominant systematic uncertainty sources are listed for each analysis based on past experiences. This is by no means a rigorous method to evaluate systematic uncertainty, which will be only possible after the detector is built, but it is a way to anticipate potential uncertainty that could arise in the analysis level. Follow-up pseudo-analysis will be performed accordingly to quantify the systematic uncertainty based on detector and physics simulations.

VII. RESULTS

In this section, we examine four selected physics channels to illustrate the scientific potential of the EIC ePIC detector during its first five years of operation. All results are reported in terms of phase I EIC luminosity; if possible, we can report the ultimate energy with higher luminosity.

A. Inclusive diffraction on nuclei

writer: Arjun, Sal + students

B. Meson Structure at the EIC

1. Meson Form Factors

Measurements of meson form factors through Deep Exclusive Meson Production (DEMP) offer insights into the internal structure of pions and their role as Goldstone bosons, which is particularly relevant for understanding the mechanism of mass generation in QCD [21]. The role the EIC can play in such studies is described in [1].

The experimental determination of F_π is challenging. The ideal method for determining F_π would be electron-pion elastic scattering. However, the lifetime of the π^+ is only 26.0 ns. Since π^+ targets are not possible, and π^+ beams with the required properties are not yet available, one must employ high-energy exclusive electroproduction, $p(e, e^{'}\pi^+ n)$. This is best described as the quasi-elastic (t-channel) scattering of the electron from the virtual π^+ cloud of the proton, where t is the Mandelstam momentum transfer $-t = -(p_p - p_n)^2$ to the target nucleon. Scattering from the π^+ cloud dominates at $|t| << m_p^2$ [22].

The ePIC Far Forward detectors are particularly important for this study. At $9(e) \times 130(p)$ beam energies, the neutrons from the DEMP reaction carry $60 - 95\%$ of the proton beam momentum and are detected in the far-forward detector region (mainly ZDC) at very forward angles ($0 - 2°$), while the scattered electrons and pions with low momenta hit the central detector over a wide range of angles. The analysis presented here only make use of the ZDC, as these events are most relevant to the low $-t$ region needed for F_π studies.

Triple coincidence $e' - \pi^+ - n$ events were selected for further analysis, with details provided in our analysis note [23]. A unique aspect of the analysis is a cut to identify exclusive events based on the difference between the calculated ($\theta_{pMiss}, \phi_{pMiss}$) trajectory of the neutron based on missing momentum information, $pMiss = p_e + p_p - p_{e'} - p_{\pi^+}$, and the actual neutron hit position on the ZDC (θ_{ZDC}, ϕ_{ZDC}). This angular difference is shown in Fig. 3a. A narrow distribution near zero demonstrates that ePIC far-forward neutron reconstruction is highly effective. Fig. 3b indicates the t reconstruction resolution using the t_{eXBABE} method which performs very well.

The detection efficiency for the triple coincidence events (see [23]) is $60 - 70\%$, and nearly independent of Q^2. It is highest for $-t < 0.15$ GeV^2, decreasing rapidly with $-t$ thereafter. Fig. 3c reflects the projected statistical uncertainties for integrated luminosities of 1 and 2.5 fb^{-1}, respectively, and the assumed systematic and model extraction uncertainties detailed in [23]. As a closing remark, the extraction of the pion form factor to high Q^2 with ePIC depends on very good ZDC angular resolution for two reasons: 1) the necessity to separate the small exclusive π^+ cross-section from dominant inclusive backgrounds via $\Delta\theta^*$ and $\Delta\phi^*$ cuts, 2) the need to reconstruct t to better than ~0.02 GeV^2, such resolution is only possible when reconstructed from the initial proton and final neutron momenta. The performance of the ePIC far forward detectors is thus of crucial importance to the feasibility of a pion form factor measurement.

2. Structure Functions

C. Imaging program of protons

1. DVCS

Deeply Virtual Compton Scattering is a golden channel for the extraction GPDs, which has been
writer: Oliver + Stephen Kay

2. DVπ^0P

Deeply virtual π^0 production (DVπ^0P) complements DVCS by accessing chiral-odd GPDs, which are suppressed in DVCS [24]. Furthermore, a recent theoretical study [25] shows that azimuthal asymmetries in this channel provide a sensitive probe for quark orbital angular momentum, the missing ingredient for understanding the nucleon spin composition.

The ePIC detector is particularly well-suited for the reconstruction of the final state in the $ep \to e'p'\pi^0(\to \gamma\gamma)$ process, where e' and p' denote the scattered electron and proton. The electron reconstruction and selection has been discussed in Section VI. The proton is detected by the B0 spectrometer, covering the polar angle $5.5 < \theta_p <$

	Dominant systematics source	Estimates
DVCS	BH interference?	
DVπ^0P	cluster merging	
DEMP	Scale uncertainty	12%
DVMP	Background estimation and efficiency	
eAu ϕ	Incoherent background and unfolding	
eHe3	Pion contamination & beam polarization	4.7%

TABLE IV: Dominant sources of systematic errors on the exclusive, diffractive and tagging measurements described in this section. These estimates are based upon past experience from the closest comparable existing measurements.

20 mrad, or the RP detector, covering the polar angle $0 < \theta_p < 5$ mrad. The two photons are detected in the mid-rapidity and forward calorimeters. The invariant mass distribution of the reconstructed π^0 candidates is shown in Fig. 4. The π^0 candidates are selected by requiring their invariant mass to be within 3σ of the nominal π^0 mass, where σ is determined from a Gaussian fit to the peak of the invariant mass distribution.

To ensure the exclusivity of the DVπ^0P process $ep \to e'p'\pi^0$, two additional selections are applied. First, the longitudinal kinematics of the final state, $E - P_z$, is required to be within the range of $15 < E-P_z < 25$ GeV. Second, the missing mass squared M_X^2 of the $ep \to e'p'\pi^0$ reaction, defined as $M_X^2 = (p_e + p_p - p_{e'} - p_{p'} - p_{\pi^0})^2$, is required to satisfy $|M_X^2| < 1$ GeV^2.

Following all these selections, the total detection efficiency of the $ep \to e'p'\pi^0$ reaction is 23%. However, 36% of signal events, in which only one photon is reconstructed mainly due to the cluster merging in the calorimeters, can be potentially recovered by implementing dedicated machine learning algorithms for future reconstruction. Additionally, signal events without a reconstructed proton, accounting for 42% of the total, can be included in the analysis by utilizing the missing mass squared spectrum of the proton, $M^2_{\text{miss }p} = (p_e + p_p - p_{e'} - p_{\pi^0})^2$.

The momentum transfer $t = (p_p - p'_p)^2$ can be directly obtained for events with a reconstructed proton, while for events without a reconstructed proton, it can be calculated using the four momentum of e' and π^0. After combining the t distributions from both event samples and applying the corrections for the acceptance and efficiency, the differential cross section as a function of $-t$ is obtained, as shown in Fig. 5 (blue open circles) together with the generator-level distribution (balck solid line). The cross section is normalized to an integrated luminosity of 1.0 fb^{-1} and the blue open circles are further smeared to match the expected statistical fluctuation.

Figure 6 shows the Fourier transform of the differential cross section $\mathrm{d}\sigma/\mathrm{d}t$, representing the quark spatial distribution within the nucleon. This result confirms the feasibility of performing the DVπ^0P analysis at the EIC with the ePIC detector.

3. DVJ/ψP

writer: Olaiya + others

D. Tagged DIS on deuteron and Helium 3

1. Spectator tagging in deuteron DIS

Proton structure functions are routinely measured in inclusive deep-inelastic scattering. However, structure functions measured on a neutron target can provide additional insight related to quark-flavor separation and enable further study into the onset of nuclear modifications to structure functions in light nuclei. Accessing neutron structure functions is experimentally challenging due to a lack of pure neutron beams/targets. A successful approach has been implemented in fixed-target experiments using spectator-tagged deep-inelastic scattering on a deuterium target, where the proton spectator is used to determine the relative momentum between the nucleons to identify a configuration where the nucleons are quasi-free [26–29]. However, the fixed-target kinematics make it difficult to achieve $p_{T,spectator} \lesssim 70$ MeV/c. In the collider kinematic environment at the EIC access to a kinematic region where $p_{T,spectator} \sim 0$ MeV/c enables application of pole extrapolation methods with smaller uncertainties to extract free neutron structure functions from the lightly bound deuteron by exploiting the behavior of the deuteron wave function near its pole [3, 30–32]. Additionally, neutron-tagged events can be used to extract free proton structure which can then be compared to measurements in electron + proton collisions with the same kinematics at the EIC, allowing for control over systematics associated with the pole extrapolation method itself.

In ePIC, simulations are performed using BeAGLE electron + deuteron DIS events passed through the full ePIC detector simulation and reconstruction framework.

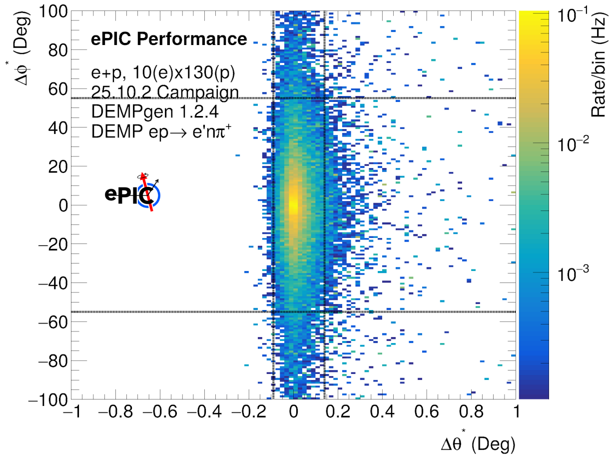

(a) $\Delta\theta^*$ vs $\Delta\phi^*$ for 10×130 events. Note that as only DEMP events are processed, the majority of events survive this cut. Cuts were chosen along lines of constant rate as the peak area of the distribution tails off, as indicated by the dashed black lines showing the cut region. Events outside of the shape confined by these four lines are removed.

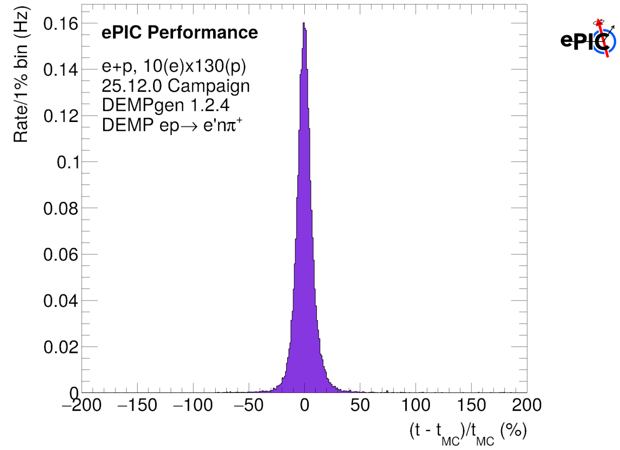

(b) A comparison of the resolution for calculated t_{eXBABE} values, defined as the deviation from the MC truth divided by the MC truth value and expressed as a percentage for 10×130 events.

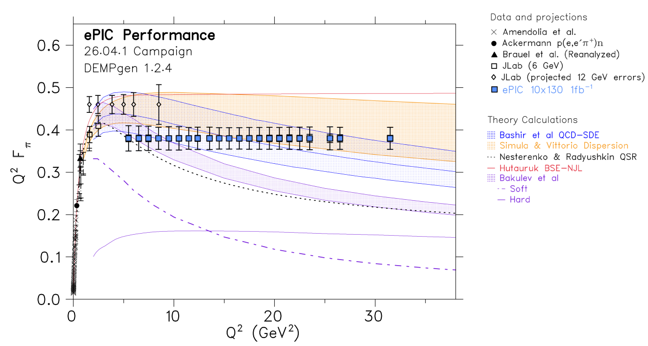

(c) Existing data and projected uncertainties for future data on the pion form factor from JLab E12-19-006 and ePIC (blue), in comparison to a variety of hadronic structure models. The projected ePIC data have double error bars, where the inner error bar includes only statistical and assumed point-to-point systematic errors, and the outer error bar includes also the correlated systematic errors. For most the ePIC data points, the statistical errors are smaller than the marker and only the total uncertainty is visible.

In the tagged-proton case, protons are reconstructed using the off-momentum detectors, while the tagged-neutron events are reconstructed using the zero-degree calorimeter.

Detailed description of the analysis procedure is available in Ref. [3], here we provide only simplified outline of the method. The first step in this analysis is extraction of the tagged-deuteron cross section $\bar{\sigma}_{\mathrm{d,red}}$. Comparison of the True MC and reconstructed (RC) $\bar{\sigma}_{\mathrm{d,red}}$ is shown in Fig. 7. In the next step, the pole of the deuteron spectral function is removed by applying the inverse of the deuteron pole factor to acquire the tagged-*nucleon* cross-section ($\bar{\sigma}_{\mathrm{red,p/n}}$).

The difference between True MC and RC, shown in Fig. 7, is caused primarily by inefficiency of the scattered electron reconstruction and by bin migration due to spectator nucleon resolution. To correct for this efficiency and acceptance, we fit True MC the tagged-*nucleon* cross-section with a linear function and the RC the tagged-*nucleon* cross-section with a third order polynomial. The correction factor is then calculated and applied bin-by-bin as a ratio of the two fit functions which allows to obtain the corrected tagged-*nucleon* cross-section, shown in Fig. 8.

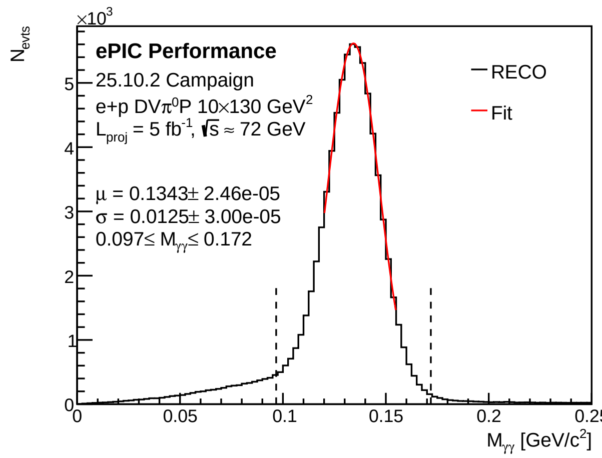

FIG. 4: Reconstructed π^0 invariant mass distribution for exclusive π^0 production. The red curve represents the Gaussian fit result and the black dashed lines indicate the $\pm 3\sigma$ selection range.(to be updated)

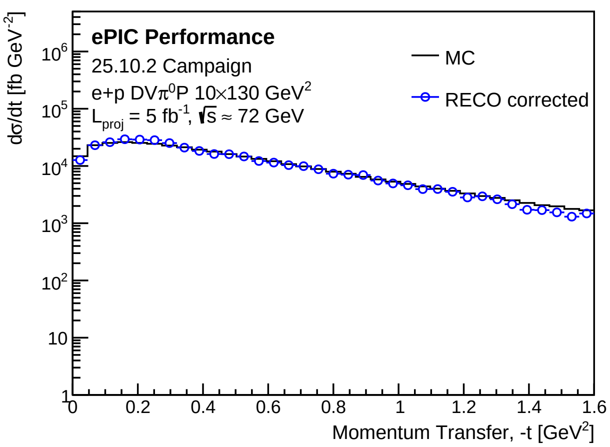

FIG. 5: Differential cross section as a function of momentum transfer $-t$ for DVπ^0P, normalized to an integrated luminosity of 1.0 fb^{-1}. The black solid line represents the generator-level distribution, while the blue open circles indicate the reconstructed distribution after acceptance and efficiency corrections.(to be updated)

Finally, a linear fit is performed to the corrected tagged-*nucleon* cross-section and the fit is evaluated at the location of pole. This extrapolated value is the reduced cross-section on the quasi-free active nucleon (tagged proton means extraction of the *neutron* reduced cross-section). The error bars in Fig. 9 are combined statistical and systematic uncertainties, where the systematic uncertainty.

The full set of these reduced cross-section values in bins of x_{bj} and for one Q^2 bin are shown in Fig. 9.

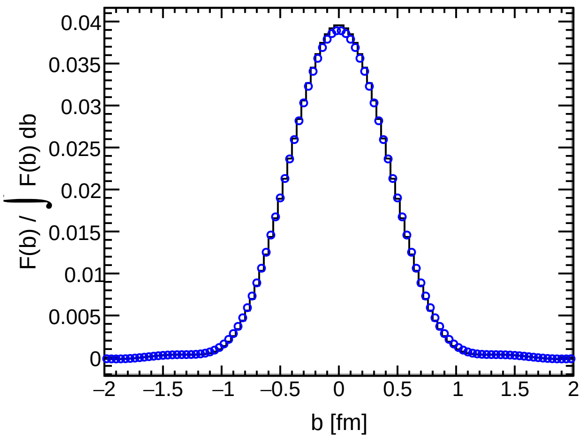

FIG. 6: Fourier transform of the differential cross-section dσ/dt, representing the quark spatial distribution. The black solid line represents the generator-level distribution, while the blue open circles indicate the reconstructed distribution after acceptance and efficiency corrections.(to be updated)

Here, the systematic and statistical uncertainties are added in quadrature and shown as error bars. Even with our conservative systematic uncertainty estimate, this simulation result clearly demonstrates the feasibility of the deuteron tagging at ePIC. The precision of analysis is expected to be dominated by the systematic uncertainties which are expected to improve significantly compared to the presented results. The statistical precision is expected to be excellent even with the expected luminosity in the early years of running of the EIC.

2. He3 with double spectator tagging

Polarized neutron measurements can be performed at EIC using a polarized ^{3}He beam. Both longitudinal and transverse polarized ^{3}He beams are expected to be available during the early stage running of EIC, enabling detailed studies of the neutron spin structure. With spectator tagging, measurements of the internal spin structure of the neutrons can achieve higher precision. In addition, the ^{3}He nuclear model can be tested by comparing tagged measurements with the fully inclusive results. A preliminary study of the impact of spectator tagging in ^{3}He has been carried out using a simple tagging algorithm and comparing the resulting virtual photon double spin asymmetry, A_1^n, with that obtained from a traditional inclusive measurement. The tagging algorithm identifies spectator protons using hit information from the Roman Pots and Off-momentum Detector. The number of proton tracks is estimated

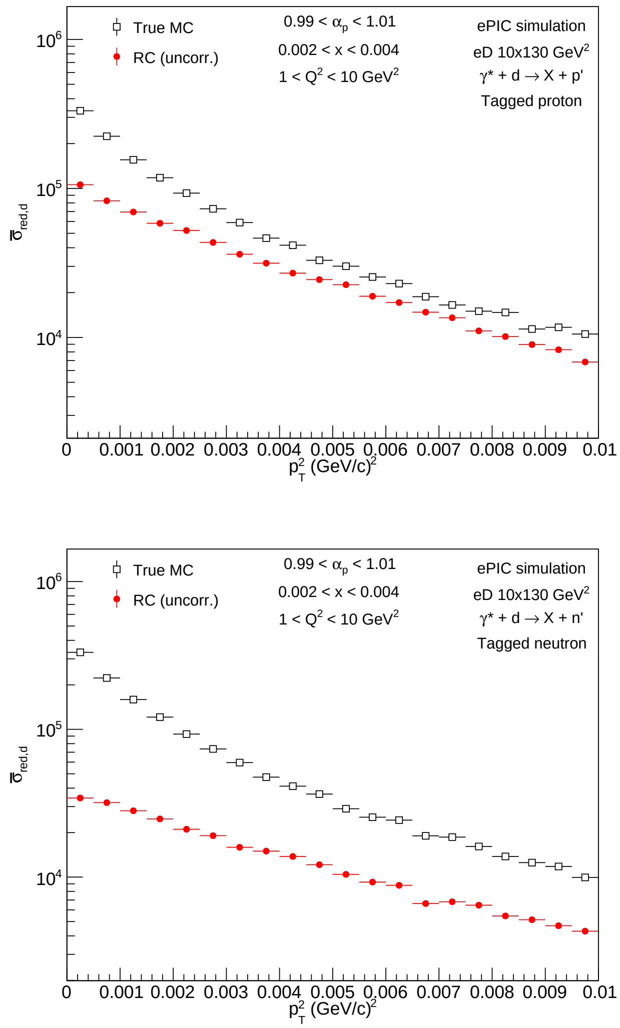

FIG. 7: Tagged-deuteron reduced cross-section from events with a tagged spectator proton (top) and neutron (bottom).

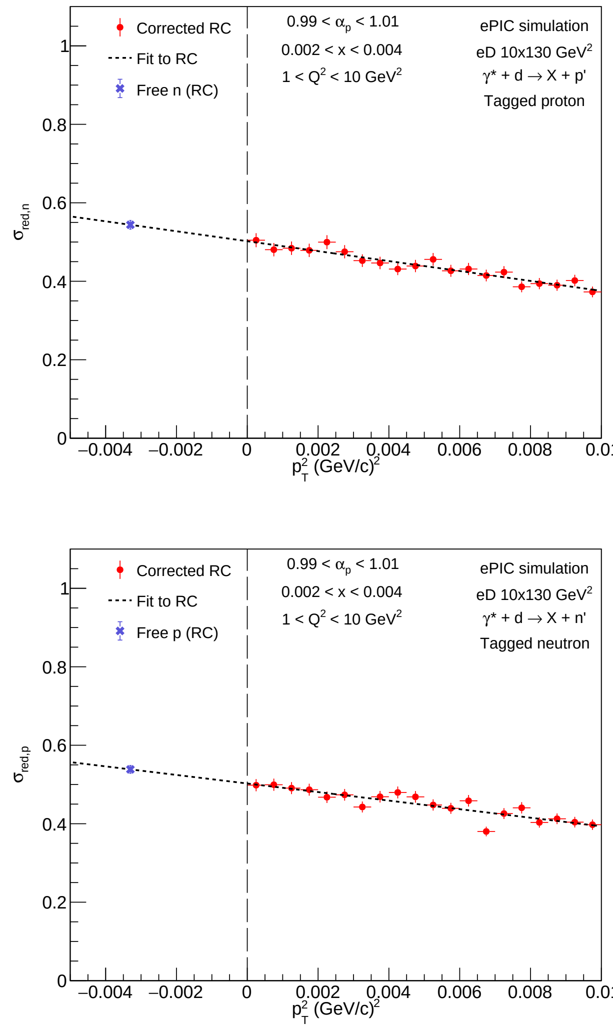

FIG. 8: Efficiency and acceptance corrected neutron (top, tagged proton) and proton (bottom, tagged neutron) cross-section after removal of pole from deuteron reduced cross-section. This distribution is then fitted with a straight line to perform the pole extrapolation to find the on-shell point where the nucleon is unbound.

from the minimum number of hits observed among the detector planes. Events with at least two reconstructed proton tracks are classified as *en* scattering candidates. Figure 10 shows the efficiency for tagging individual spectator protons using the current tagging algorithm. The bending of the proton trajectory in the far-forward region is characterized by the longitudinal momentum fraction, $x_L = p_{z,\,\mathrm{proton}}/p_{z,\,\mathrm{beam}}$, with lower x_L protons bending more strongly toward the OMD. The dip in efficiency around x_L of 0.33 is caused by the gap between the OMD and the RP. The spectator tagging efficiency in e^3He scattering can be further improved by optimizing the positions of the OMD and RP in the far-forward detector system.

Figure. 11 illustrates the potential improvement in the uncertainty of A_1^n by applying double spectator tagging. The uncertainties shown include both the statistical uncertainty and the model uncertainty associated with the structure functions. For the traditional extraction of A_1^n from inclusive DIS measurements, a simple ^{3}He model is employed:

$$A_1^{^3\mathrm{He}} = P_n \frac{F_2^n}{F_2^{^3\mathrm{He}}} A_1^n + 2P_p \frac{F_2^p}{F_2^{^3\mathrm{He}}} A_1^p. \tag{1}$$

In this model, $A_1^{^3\mathrm{He}}$, A_1^p and A_1^n denote the spin asymmetries for ^{3}He, the proton, and the neutron, respectively. The effective nucleon polarizations in ^{3}He are $P_n = 0.86 \pm 0.02$ and $P_p = -0.028 \pm 0.004$ [33]. $F_2^{^3\mathrm{He}}$, F_2^p and F_2^n are the corresponding unpolarized structure

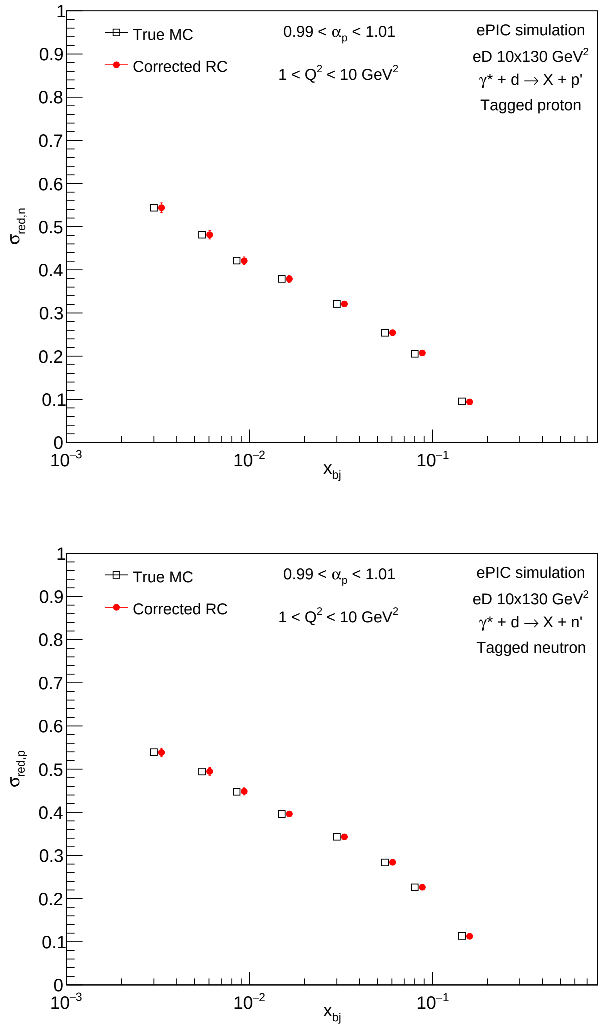

FIG. 9: Summary of the neutron (top, tagged proton) and proton (bottom, tagged neutron) reduced cross-sections extracted from the pole extrapolation procedure in x_{bj} bins. These are all evaluated for the electron + deuteron luminosity expected during the early EIC running period.

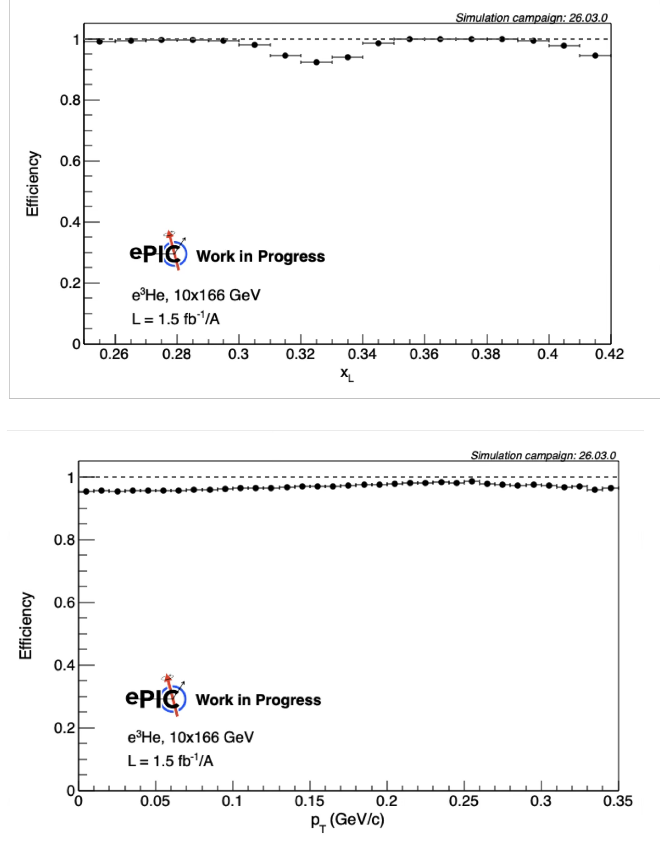

FIG. 10: Efficiency of tagging individual spectator protons in e^3He scattering. Top: tagging efficiency as a function of the spectator proton longitudinal momentum fraction in ^{3}He. Bottom: tagging efficiency as a function of the spectator proton transverse momentum.

functions. For the projection study, the asymmetries are taken from parameterizations [34], and the structure functions are taken from the JAM22 global fit [35]. Comparing the two extraction methods, the double tagging approach reduces the total uncertainty on A_1^n by approximately 50% to 70%, depending on the kinematic region.

E. Imaging program of heavy nuclei and saturation physics

The momentum transfer distribution ($|t|$) forms a diffractive pattern that encodes information about the spatial distribution of gluons in the hadron wave function [36]. Since $|t|$ is conjugate to the impact parameter, a Fourier-Bessel (Hankel) transformation of the distribution enables us to obtain the spatial profile of the gluon density. Experimentally, however, measuring the $|t|$ distribution for heavy nuclei is challenging because it requires precise knowledge of the outgoing nucleus momentum—information that cannot be obtained directly, since diffracted heavy nuclei remain inside the beam envelope. This limitation necessitates alternative reconstruction techniques. Two major complications arise: (1) limited momentum resolution, and (2) significant background from incoherent events in which the nucleus breaks up. Measuring the diffractive pattern of the $|t|$ distribution from coherent VM production as well as from UPCs has been studied previously at different facilities such as HERA, JLab, RHIC etc. [37–39]. These studies have established the foundational understanding of the $|t|$ dependence, but their ability to resolve the full diffractive pattern has been limited. This analysis utilizes a projective technique ($|t|_{\omega_{\max}}$), as demonstrated in [4], to reconstruct

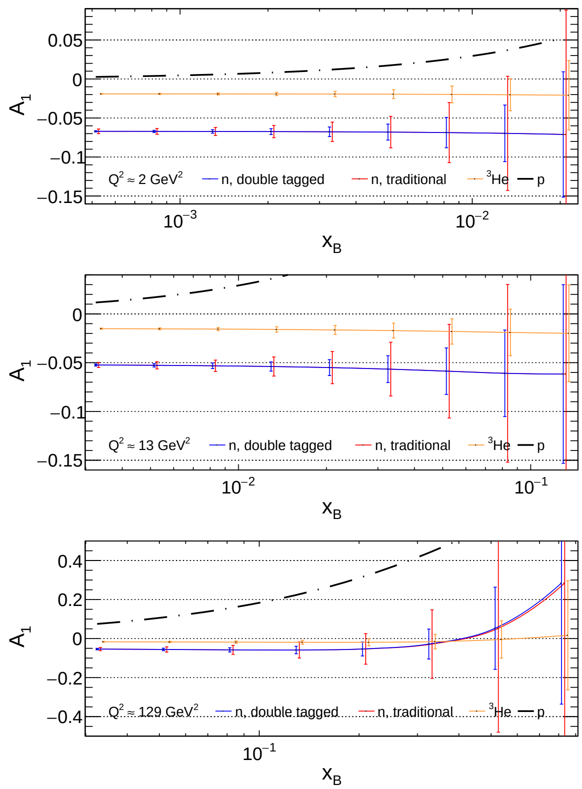

FIG. 11: Comparison of A_1^n uncertainties extracted using the traditional model dependent method (blue) versus the double tagging method (red) at three selected Q^2 bin. The orange line in each plot is the estimated statistical uncertainty of $A_1^{^3\mathrm{He}}$ while the black dashed line is the central value of A_1^p.

the $|t|$ distribution by invoking cuts and momentum projection along the direction normal to the electron scattering plane ($\hat{n}$) to resolve the diffractive pattern and the resulting gluon distribution through a Fourier-Bessel transformation. More information about the analysis procedure can be found in the analysis note [40].

Previously, the best method for $|t|$ reconstruction through exclusive VM production was using the $|t|_{\mathrm{eXBE}}$ method [1]. The $|t|_{\omega_{\max}}$ method incorporates a projection and a wedge cut as an additional requirement for $|t|_{\mathrm{eXBE}}$ reconstruction. Following [4], we take the projection of $|t|$ to the $\hat{n}$ direction to reduce the momentum resolution contribution from the scattered electron. This projection is accomplished by first determining the $|t|_{\hat{n}}$ component defined by

$$\begin{aligned} |t|_{\hat{n}} &= [(e - e' - p_{\mathrm{VM}}) \cdot \hat{n}]^2 \\ &= (p_{\mathrm{VM}} \cdot \hat{n})^2, \end{aligned} \tag{2}$$

where the components are now $|t|_{\mathrm{proj}} = (|t|_E, |t|_x, |t|_{\hat{n}}, |t|_z)$. Given the relation $|t|_\perp = \Delta_\perp^2 = \Delta_x^2 + \Delta_y^2$, we decompose the transverse components such that $\Delta_x = \sqrt{|t|_x}$ and $\Delta_y = \sqrt{|t|_{\hat{n}}}$. Note that for heavy nuclei $t_\parallel \ll t_\perp$ [41] and is neglected in this analysis. We then parameterize Δ_x and Δ_y in terms of ω and cut a wedge of angle $\omega_{\max}$ defined by

$$\omega_{\max} = \tan^{-1}\left(\sqrt{\frac{|t|_x}{|t|_{\hat{n}}}}\right), \tag{3}$$

to emphasize the phase space where $|t|_{\hat{n}}$ is dominate (see [4] for more details). This process allows us to eliminate most of the momentum resolution contribution from the scattered electron.

After constructing the momentum transfer profile as described above, we can take a Fourier-Bessel transformation to extract the spatial distribution of the gluons [5]. As shown in [42], a 2-dimensional transformation of the transverse $|t|$ distribution gives the transverse distribution of the spatial profile. The transformation used is given by

$$F(b) \propto \frac{1}{2\pi} \int_0^\infty d\Delta_\perp \Delta_\perp J_0(b\Delta_\perp) \sqrt{\frac{d\sigma}{d|t|}}, \tag{4}$$

where J_0 is a Bessel function of the first kind, b is the impact parameter, and $d\sigma/d|t|$ is the differential cross section. The diffractive pattern of the $|t|$ distribution as well as the transformation allow us to study the onset of gluon saturation.

The results of this reconstruction are shown in Fig. 12. First, we can see a significant enhancement in resolving the diffractive pattern of the $|t|$ distribution. The projection method enables us to determine the peaks and minima with a much better resolution than before. The price we pay for making the wedge cut in the projection method is a loss of statistics, as shown in Fig. 12. In this example, we use $\omega_{max} = \pi/12$ which results in $\approx 83\%$ of lost coherent VM events. Second, the transformation shown in Fig. 12 clearly indicates an improvement the transformation of the $|t|$ distribution. The distribution extracted by the STAR experiment for ρ^0 [39] is shown for comparison with the truth and projected distribution. This shows the importance of precisely determining the minima of the diffractive pattern in the $|t|$ distribution to retrieve an accurate transformation to the spatial profile of the gluons.

In future work, we intend to study the impact of different machine backgrounds such as synchrotron radiation [43]. Furthermore, we will test the projection technique at different energies beyond the early science configurations for comparison. Additionally, we will study background removal utilizing both longitudinal and transverse polarization. Since there is no transverse polarization during the early science period, this component will applicable at a later stage in EIC running. This analysis demonstrates that the projection method used to reconstruct the momentum distribution is an effective approach to overcome the previous limitations of the $|t|$ measurement and enables more precise spatial imaging of the gluons inside the nucleus.

VIII. SUMMARY

This paper presents the early science prospects for the exclusive physics program during Phase I of the Electron-Ion Collider (EIC). The focus is on leveraging high-luminosity electron-proton and electron-nucleus collisions to explore the fundamental structure of hadrons and nuclei through exclusive processes. These reactions, where all final-state particles are measured, offer clean access to the underlying dynamics of strong interactions.

The Phase I running plan provides a diverse range of beam species, energies, and polarization configurations, enabling precision studies of exclusive reactions across a wide kinematic range. Light nuclei, such as deuterium and helium-3, allow for unique probes of nucleon and nuclear structure, while heavy ions like gold facilitate studies of coherence and diffractive phenomena.

The paper outlines the expected experimental conditions and integrated luminosities, along with simulation-based projections that demonstrate the feasibility and impact of the early exclusive measurements. These results will lay the groundwork for the EIC's long-term physics goals and help establish the collider as a leading facility for exploring the quantum structure of matter.

ACKNOWLEDGMENTS

The ePIC Collaboration would like to thank... *we need official acknowledgment from the ePIC management*

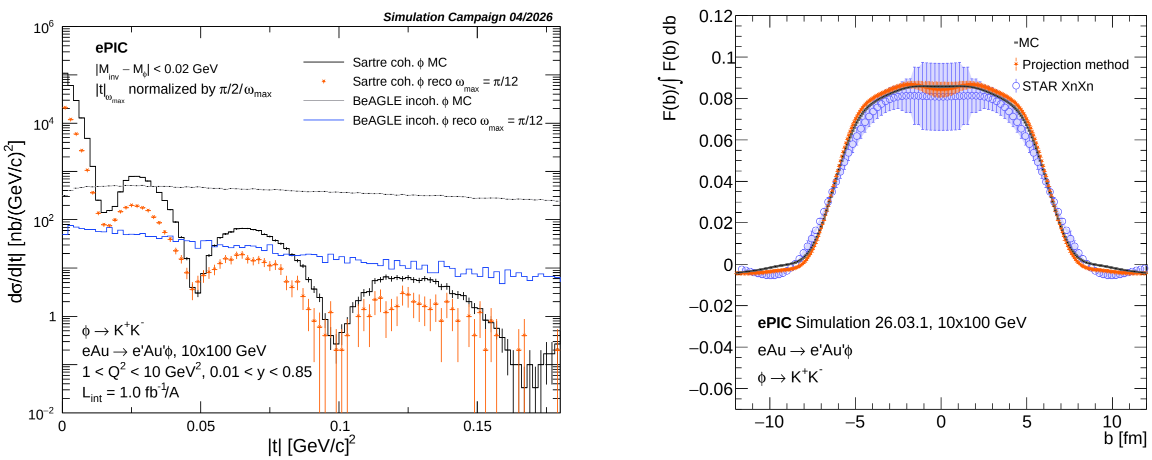

FIG. 12: Left: $|t|$ distribution with both $|t|_{\omega_{\max}}$ (orange stars) and $|t|_{\mathrm{MC}}$ (black curve). The $|t|_{\omega_{\max}}$ reconstruction corresponds to a wedge cut of $\omega_{\max} = \pi/12$. See Section VII E and [4] for more details. Note that the $|t|_{\omega_{\max}}$ distribution is normalized by $(\pi/2)/\omega_{\max}$ Right: 2-dimensional Fourier-Bessel transformation of the $|t|$ distribution. This shows the gluon spatial distribution with a comparison from the transforms of $|t|_{\mathrm{MC}}$, $|t|_{\omega_{\max}}$, and $|t|_{XnXn}$ reconstructed from STAR data [39].

[1] R. A. et. al, Science requirements and detector concepts for the electron-ion collider: Eic yellow report, Nuclear Physics A **1026**, 122447 (2022).
[2] ePIC, Inclusive physics opportunities at the ePIC experiment in the early stage of EIC.
[3] A. Jentsch, Z. Tu, and C. Weiss, Deep-inelastic electron-deuteron scattering with spectator nucleon tagging at the future Electron Ion Collider: Extracting free nucleon structure, Phys. Rev. C **104**, 065205 (2021), arXiv:2108.08314 [hep-ph].
[4] M. Kesler, A. I. Sheikh, R. Ma, Z. Tu, T. Ullrich, and Z. Xu, Projective imaging of high-energy nuclei via coherent exclusive vector meson production in electron-nucleus collisions, Physics Letters B , 140585 (2026).
[5] T. Toll and T. Ullrich, Exclusive diffractive processes in electron-ion collisions, Phys. Rev. C **87**, 024913 (2013), arXiv:1211.3048 [hep-ph].
[6] T. Toll and T. Ullrich, The dipole model Monte Carlo generator Sar*t*re 1, Comput. Phys. Commun. **185**, 1835 (2014), arXiv:1307.8059 [hep-ph].
[7] W. Chang, E.-C. Aschenauer, M. D. Baker, A. Jentsch, J.-H. Lee, Z. Tu, Z. Yin, and L. Zheng, Benchmark eA generator for leptoproduction in high-energy lepton-nucleus collisions, Phys. Rev. D **106**, 012007 (2022), arXiv:2204.11998 [physics.comp-ph].
[8] W. Chang, E.-C. Aschenauer, M. D. Baker, A. Jentsch, J.-H. Lee, Z. Tu, Z. Yin, and L. Zheng, Investigation of the background in coherent J/ψ production at the EIC, Phys. Rev. D **104**, 114030 (2021), arXiv:2108.01694 [nucl-ex].
[9] Z. Tu, A. Jentsch, M. Baker, L. Zheng, J.-H. Lee, R. Venugopalan, O. Hen, D. Higinbotham, E.-C. Aschenauer, and T. Ullrich, Probing short-range correlations in the deuteron via incoherent diffractive J/ψ production with spectator tagging at the EIC, Phys. Lett. B **811**, 135877 (2020), arXiv:2005.14706 [nucl-ex].
[10] C. M. Robles Gajardo, A. Accardi, M. D. Baker, W. K. Brooks, R. Dupré, M. Ehrhart, J. A. López, and Z. Tu, Low energy protons as probes of hadronization dynamics, Phys. Rev. C **106**, 045202 (2022).
[11] T. Sjöstrand, S. Mrenna, and P. Skands, PYTHIA 6.4 Physics and Manual, JHEP (2006) **05**, 026, arXiv:hep-ph/0603175 [hep-ph].
[12] T. Böhlen, F. Cerutti, M. Chin, A. Fassò, A. Ferrari, P. Ortega, A. Mairani, P. Sala, G. Smirnov, and V. Vlachoudis, The FLUKA Code: Developments and Challenges for High Energy and Medical Applications, Nucl. Data Sheets **120**, 211 (2014).
[13] A. Ferrari, P. R. Sala, A. Fasso, and J. Ranft, FLUKA: A multi-particle transport code (Program version 2005), SLAC-R-773, 10.2172/877507 (2005).
[14] Z. Ahmed, R. Evans, I. Goel, G. Huber, S. Kay, W. Li, L. Preet, and A. Usman, Dempgen: Physics event generator for deep exclusive meson production at jefferson lab and the eic, Computer Physics Communications **308**, 109444 (2025).
[15] S. Joosten, *Argonne l/A-event Generator* (GitLab repository, 2021).
[16] E. C. Aschenauer, V. Batozskaya, S. Fazio, K. Gates, H. Moutarde, D. Sokhan, H. Spiesberger, P. Sznajder, and K. Tezgin, EpIC: novel Monte Carlo generator for exclusive processes, Eur. Phys. J. C **82**, 819 (2022), arXiv:2205.01762 [hep-ph].
[17] `https://pawelsznajder.github.io/epic/`.
[18] B. Berthou *et al.*, PARTONS: PARtonic Tomography Of Nucleon Software: A computing framework for the phenomenology of Generalized Parton Distributions, Eur. Phys. J. C **78**, 478 (2018), arXiv:1512.06174 [hep-ph].
[19] `https://partons.cea.fr/partons/doc/html/index.html`.
[20] E. C. Aschenauer, V. Batozskaya, S. Fazio, A. Jentsch, J. Kim, K. Kumerički, H. Moutarde, K. Passek-K., D. Sokhan, H. Spiesberger, P. Sznajder, and K. Tezgin, Study of deeply virtual compton scattering at the future electron-ion collider, Phys. Rev. D **112**, 036010 (2025), arXiv:2503.05908 [hep-ph].
[21] J. Arrington *et al.*, Revealing the structure of light pseudoscalar mesons at the electron–ion collider, Journal of Physics G: Nuclear and Particle Physics **48**, 075106 (2021).
[22] C. E. Carlson and J. Milana, Difficulty in determining the pion form factor at high q^2, Phys. Rev. Lett. **65**, 1717 (1990).
[23] G. Huber, S. Kay, and L. Preet, *epic-AN-AC-2026-02: Light Meson Form Factors from Deep Exclusive Meson Production in early EIC science configurations with the ePIC Detector* (2026).
[24] M. Diehl, Generalized parton distributions with helicity flip, Eur. Phys. J. C **19**, 485 (2001), arXiv:hep-ph/0101335.
[25] S. Bhattacharya, D. Zheng, and J. Zhou, Probing the Quark Orbital Angular Momentum at Electron-Ion Colliders Using Exclusive π0 Production, Phys. Rev. Lett. **133**, 051901 (2024), arXiv:2312.01309 [hep-ph].
[26] A. V. Klimenko *et al.* (CLAS), Electron scattering from high-momentum neutrons in deuterium, Phys. Rev. **C73**, 035212 (2006), arXiv:nucl-ex/0510032 [nucl-ex].
[27] N. Baillie *et al.* (CLAS), Measurement of the neutron F2 structure function via spectator tagging with CLAS, Phys. Rev. Lett. **108**, 142001 (2012), [Erratum: Phys.Rev.Lett. 108, 199902 (2012)], arXiv:1110.2770 [nucl-ex].
[28] S. Tkachenko *et al.* (CLAS), Measurement of the structure function of the nearly free neutron using spectator tagging in inelastic ^{2}H(e, e'p)X scattering with CLAS, Phys. Rev. C **89**, 045206 (2014), [Addendum: Phys.Rev.C 90, 059901 (2014)], arXiv:1402.2477 [nucl-ex].
[29] S. Bueltmann *et al.*, The Structure of the Free Neutron at Large x-Bjorken, Report JLAB-PR12-06-113, `https://www.jlab.org/exp_prog/proposals/10/PR12-06-113-pac36.pdf` (2006).
[30] M. Sargsian and M. Strikman, Model independent method for determination of the dis structure of free neutron, Physics Letters B **639**, 223 (2006).
[31] M. Strikman and C. Weiss, Electron-deuteron deep-inelastic scattering with spectator nucleon tagging and final-state interactions at intermediate x, Phys. Rev. C **97**, 035209 (2018).
[32] W. Cosyn and C. Weiss, Polarized electron-deuteron deep-inelastic scattering with spectator nucleon tagging,

Phys. Rev. C **102**, 065204 (2020), arXiv:2006.03033 [hep-ph].

[33] F. Bissey, A. W. Thomas, and I. R. Afnan, Structure functions for the three-nucleon system, Phys. Rev. C **64**, 024004 (2001).

[34] X. Zheng *et al.* (Jefferson Lab Hall A Collaboration), Precision measurement of the neutron spin asymmetries and spin-dependent structure functions in the valence quark region, Phys. Rev. C **70**, 065207 (2004).

[35] C. Cocuzza, W. Melnitchouk, A. Metz, and N. Sato (Jefferson Lab Angular Momentum (JAM) Collaboration), Polarized antimatter in the proton from a global QCD analysis, Phys. Rev. D **106**, L031502 (2022).

[36] N. Armesto and A. H. Rezaeian, Exclusive vector meson production at high energies and gluon saturation, Phys. Rev. D **90**, 054003 (2014), arXiv:1402.4831 [hep-ph].

[37] A. Bruni, X. Janssen, and P. Marage, Exclusive Vector Meson Production and Deeply Virtual Compton Scattering at HERA, arXiv e-prints , arXiv:0812.0539 (2008), arXiv:0812.0539 [hep-ph].

[38] M. Paolone, Coherent ϕ Production on Nuclei at JLab and Beyond, in *Next Generation Nuclear Physics with JLab12 and the EIC* (Workshop, 2016) p. 2.

[39] L. Adamczyk *et al.* (STAR), Coherent diffractive photoproduction of ρ^0mesons on gold nuclei at 200 GeV/nucleon-pair at the Relativistic Heavy Ion Collider, Phys. Rev. C **96**, 054904 (2017), arXiv:1702.07705 [nucl-ex].

[40] M. Kesler, A. I. Sheikh, R. Ma, Z. Tu, T. Ullrich, and Z. Xu, Analysis note: Precision extraction of momentum transfer in diffractive coherent exclusive vector meson production (2026).

[41] M. Lomnitz and S. Klein, Exclusive vector meson production at an electron-ion collider, Phys. Rev. C **99**, 015203 (2019), arXiv:1803.06420 [nucl-ex].

[42] L. Adamczyk *et al.* (STAR Collaboration), Coherent diffractive photoproduction of ρ^0 mesons on gold nuclei at 200 gev/nucleon-pair at the relativistic heavy ion collider, Phys. Rev. C **96**, 054904 (2017).

[43] A. Natochii, A new framework for synchrotron radiation studies in the eic experiment (2024).